Observation of a quasi-one-dimensional variation of the Stern-Gerlach effect

K. S. Melin, P. I. Nagornykh, Y. Lu, L. E. Hillberry, Y. Xu, and M. G. Raizen*

Center for Nonlinear Dynamics and Department of Physics, The University of Texas at Austin, Austin, Texas 78712, USA

(Received 17 December 2018; published 18 June 2019)

We report the demonstration of a quasi-one-dimensional Stern-Gerlach effect on a supersonic beam of lithium-7 atoms. This method combines a pulsed magnetic field gradient plus a strong bias field to create a quasi-one-dimensional force. We discuss the application of this technique to a cooling method and earth-based microgravity experiments.

DOI: 10.1103/PhysRevA.99.063417

The deflection of an atomic beam in an inhomogeneous magnetic field, known as the Stern-Gerlach effect, is a textbook experiment [1] at the foundation of modern physics. In the original work [2], performed by Otto Stern and Walter Gerlach in 1922, a collimated beam of silver atoms was passed through a permanent, spatially varying magnetic field. The deflected trajectories, detected on a screen downstream, showed two distinct lines, thereby demonstrating the quantized nature of atomic angular momentum and the existence of electron spin. The effect has since found applications in atom optics [3–9], atom interferometry [10,11], and isotope separation [12]. The collimating slit used in the original experiment minimized the beam divergence expected from Maxwell's equations, which forbid a purely one-dimensional magnetic field gradient. Creating a one-dimensional Stern-Gerlach effect has practical implications for the ability to control atoms with magnetic fields [13] and the design of "flat" mirrors capable of reflecting particles specularly without the dispersion of wave vectors [3–5]. Additionally, the proposed method of magneto-optical cooling, which relies on cycles of optical pumping and one-dimensional pulsed magnetic kicks, will compress atomic phase space one dimension at a time without loss of atoms [14]. Another exciting application is the ability to simulate microgravity conditions. Using a one-dimensional force to cancel gravity, one may conduct noncontact studies of levitated magnetic nanoparticles, improve loading of atoms into optical dipole traps [15], and further research of cold atoms in force-free environments without leaving Earth [16].

A one-dimensional Stern-Gerlach effect can be created if we consider a cloud of atoms, each with a magnetic dipole moment $\boldsymbol{\mu}$ in the presence of a spatially dependent magnetic field $\mathbf{B}(\mathbf{r})$. Atoms will experience the combination of rectilinear motion and precession of the magnetic moment caused by the force $\nabla(\boldsymbol{\mu}\cdot\mathbf{B})$ and torque $\boldsymbol{\mu}\times\mathbf{B}$, respectively. For sufficiently fast precession ($\gtrapprox$100 MHz for fields greater than 10 G), an adiabatic approximation is valid in which the magnetic moment is taken as always parallel to the magnetic field. In this approximation the average force $\mathbf{F}=\mu\nabla|\mathbf{B}|$ determines the motion of each atom, which indicates the existence of magnetic field configurations that provide an approximately one-dimensional kick over the finite extent of the atomic cloud. One such configuration was considered in the design of magnetic mirrors [4,6]. An alternative configuration that we employ is the sum of a strong bias field and a gradient. In this case, as long as the size of the atomic cloud d satisfies the condition $|d\nabla B|\ll B_{\text{bias}}$, where $B=|\mathbf{B}|=|\mathbf{B}_{\text{bias}}+\mathbf{B}_{\text{gadient}}|$ and $B_{\text{bias}}=|\mathbf{B}_{\text{bias}}|$, then all atoms in the cloud experience the same force and undergo a *one-dimensional* kick. Additionally, for an atomic beam experiment like the original Stern-Gerlach demonstration, the above condition is not satisfied when the cloud enters or exits the field region. One straightforward solution to this problem is to pulse the fields only while the cloud is centered in the kicking region.

In this paper we demonstrate a quasi-one-dimensional Stern-Gerlach effect on a supersonic beam of lithium-7 atoms with a pulsed magnetic field gradient plus a strong bias.

A schematic of our experiment is shown in Fig. 1(a). The starting point is a supersonic nozzle that produces an 8-μs helium pulse at a repetition rate of 0.33 Hz. To increase the interaction time of the beam with the upcoming magnetic kick, we reduce the mean velocity of the helium to 480 m/s by lowering the nozzle temperature to 18 K with a cryocooler. Lithium is seeded into the resulting helium pulse via a directional effusive oven [17] maintained at 550 °C. As the helium expands, the lithium mixes and assumes the temperature and spatial profile of the helium. After passing through a 5-mm skimmer, placed 17.5 cm away from the nozzle, the flux of Li is $\approx 10^{10}$ atoms/pulse and has a longitudinal temperature of 200 mK.

Prior to applying a magnetic kick, we prepare both the phase space and the internal state of the lithium for optimal detection. The transverse components of the phase space are set by an additional 5-mm pinhole placed 44 cm away from the nozzle. This results in a clipped beam with a transverse temperature of $\approx$4 mK and a flux of $\approx 10^7$ atoms/pulse.

The longitudinal phase space and internal state of the lithium are prepared between the skimmer and the pinhole. First, all atoms are optically pumped into the $2S_{1/2}$ $F=2$ state. Then, by applying a 15-μs laser pulse, a thin slice near the center of the cloud is selected for imaging by transferring it to the $2S_{1/2}$ $F=1$ high-field-seeking state. All optical transitions operate on the 671-nm $D1$ line with laser intensities above saturation.

*raizen@physics.utexas.edu

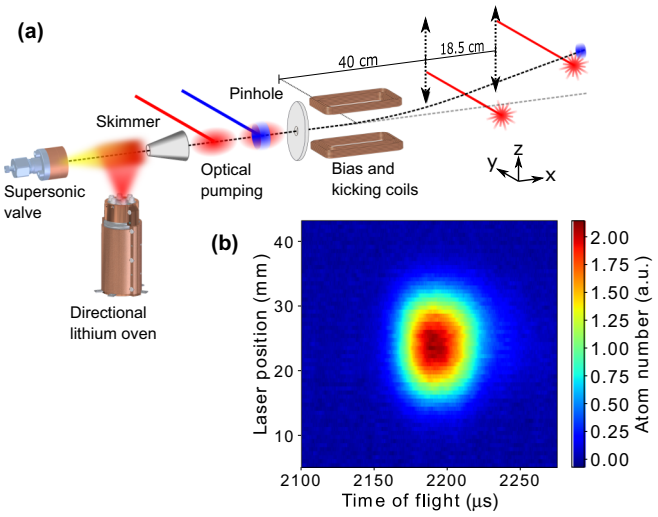

FIG. 1. Schematic of the experimental setup with a sample time-of-flight dataset. (a) Supersonic helium is released from the pulsed nozzle and seeded with lithium vapor from a directional effusive oven. The skimmer, optical pumping lasers, and pinhole prepare the internal state and phase space of the lithium before being kicked by pulsed electromagnets. Fluorescence imaging detects the sample at one of two points along the x axis. Both detection lasers can be scanned along the z axis. (b) Sample of acquired time-of-flight fluorescence of lithium over laser scan range.

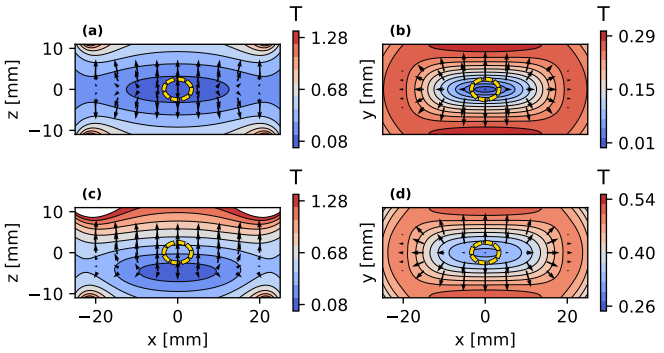

FIG. 2. Simulation of the magnetic field. Contour plots of the norm of the magnetic field are overlaid by a vector plot to indicate the direction and strength of the magnetic force on high-field-seeking atoms. Axes correspond with the coordinate system shown in Fig. 1. The dotted yellow region represents the extent of the lithium cloud at the peak of the magnetic kick. [(a), (b)] Only the anti-Helmholtz coils are active at 1500 A, producing a symmetric field and force profile about the axis of propagation. [(c), (d)] An additional 1800-A bias coil has been included which shifts the field zero point off the propagation axis and weakens xy dispersion. The result is a uniform force in the region of the atoms.

After exiting the pinhole, the beam travels for 6 cm before entering the kicking region. Here, two pairs of square, coaxial coils are oriented orthogonal to the propagation axis of the atoms. Coil dimensions were chosen to satisfy the competing criteria of maximizing field uniformity along the propagation axis while minimizing the inductance of the coils which lengthens the pulse duration. The smaller, 43.0 mm×20.3 mm, inner coils function as a pulsed anti-Helmholtz pair that creates a strong magnetic field gradient. The larger, 50.0 mm×28.4 mm, outer coils are pulsed individually to provide a magnetic bias of either sign. For any particular experiment three coils are pulsed. Using a single-bias coil also adds a gradient; however, it is relatively small compared to that produced by the inner pair. All four coils are 2×6 layers of 20 American wire gauge (AWG) wire and both pairs are separated by 26.4 mm. We avoid generating bias fields via a standard Helmholtz pair configuration because neighboring concentric inner and outer coils are strongly coupled by mutual inductance which inflicts severe current imbalances. The large current pulses required to kick the atoms are generated with custom circuitry to produce 100-μs half-sine current profiles which reach peak currents of 1.7 kA.

Cross sections of the norm of the peak magnetic field and corresponding force vectors for high-field-seeking atoms are shown in Fig. 2. In the absence of the bias coil and at a kicking current of 1.5 kA, shown in Figs. 2(a) and 2(b), the cloud, which is expected to pass within the dotted yellow line, will be pulled apart in all three dimensions. Adding one of the bias coils at 1.8 kA shifts the field zero point by 5 mm from the center as seen in Fig. 2(c). Additionally, the gradient in the xy plane is flattened, resulting in a weaker off-axis force shown in Fig. 2(d). This produces a uniform force along the z axis, a weak dispersing force in the xy plane, and hence a nearly one-dimensional magnetic kick.

We measure the shape and position of the lithium cloud at two propagation distances after the kick (40 and 58.5 cm from the coils) by focusing a fluorescence signal from the kicked $2S_{1/2}F = 1$ atoms onto one of two avalanche photodiodes. Measuring the cloud at two locations allows us to distinguish magnetic focusing and defocusing [9] from thermal heating of the cloud due to inhomogeneities of the kick.

The fluorescence data are gathered by illuminating the atoms with laser light tuned to the $F = 1 \rightarrow F' = 2$ transition. A full picture of the transverse cloud shape is collected by translating the detection lasers (with spot size of about 2 mm) perpendicular to the atomic beam after each pulse. The time-of-flight fluorescence signal from each slice is then combined to produce two-dimensional scans like the example shown in Fig. 1(b). Because this measurement integrates the fluorescence signal along the laser beam propagation direction, it is insensitive to spatial variations of the cloud shape along the laser. These transverse effects are captured in additional data sets collected after rotating the coils by 90 deg around the atomic beam axis. This allows us to align the kick either parallel or orthogonal to the scan axis of the laser and hence image both the z and y directions with the laser scan while time-of-flight data provide information about the x direction.

While holding the anti-Helmholtz coils at a fixed peak pulsing voltage of 600 V, we sweep the voltage of the bias coils individually to characterize the effects of the bias field strength and direction on the behavior of the lithium cloud. The bias range of ±800 V is set due to the limits of the circuitry. At higher voltages, noise generated from sinking large currents begins to interfere with the low-power timing circuitry.

All of the collected time-of-flight scans are analyzed by fitting a two-dimensional Gaussian distribution to extract the

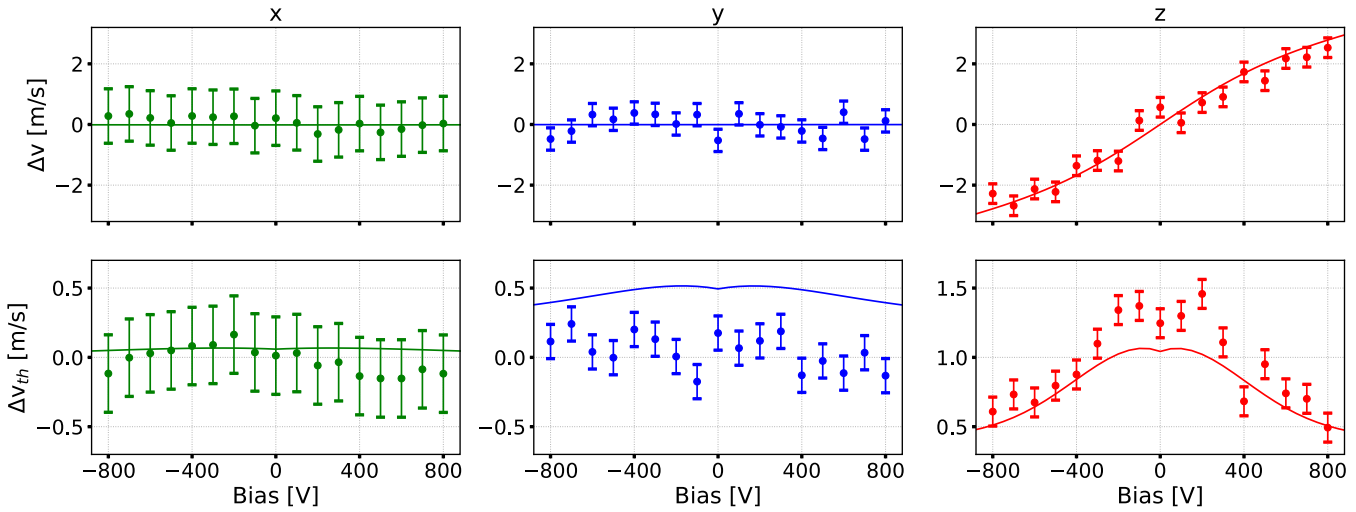

FIG. 3. Dependence of the changes in velocity and thermal velocity of the lithium atoms on bias voltages in three dimensions. Coordinate axes correspond to those shown in Fig. 1. The changes in velocity are reported relative to the beam with no magnetic fields present. The kicking gradient is oriented along the z axis and the solid lines correspond to simulation results.

center displacement of the cloud and its width, defined as the 1σ deviation from the cloud center. The results from both lasers are combined to convert center displacements into cloud velocities and widths into thermal velocities. We then subtract the results of the same analysis but with all coils off (see Fig. 3). This allows us to present our experimental data in a form that is independent of the propagation distance after the kick.

As expected, no kick is observed at zero bias, but as the magnitude of the bias voltage is increased, stronger kicks are observed along the z axis. A maximum kick of $\Delta v = 2.5 \pm 0.3\,(-2.3 \pm 0.3)$ m/s at $+800$ (-800) V bias has been achieved, constrained only by the limits of the electronics. Kicks along the other two axes remain small over all voltages with kicks not exceeding 0.5 m/s. Because of the bias configuration employed, saturation of the kick will not occur in our system since the single bias coil will always produce an additional gradient, resulting in an associated kick on the cloud.

To estimate whether the kick is truly one-dimensional, it is necessary to confirm that nonzero kicks lead to a small (zero for a true one-dimensional kick) change in thermal velocity, $\Delta v_{\rm th}$, in all directions. The thermal velocity of the cloud is evaluated from the width of the cloud via a standard time-of-flight analysis,

$$v_{th} = \sqrt{\frac{k_{\rm B}T}{m}} = \sqrt{\frac{\sigma_2^2 - \sigma_1^2}{t_2^2 - t_1^2}}$$

where $k_{\rm B}$ is the Boltzmann constant, m is the mass of lithium atom, T is the transverse temperature, and $\sigma_{1,2}$ are the transverse widths of the lithium cloud at times $t_{1,2}$ since passing the skimmer. As a function of bias voltage, $\Delta v_{\rm th}$ is shown in Fig. 3 for all axes. Kicking along the z axis, the change in thermal velocity peaks near low biases at 1.2 ± 0.1 m/s and tapers off at high biases to 0.5 ± 0.1 m/s at $+800$ V and 0.6 ± 0.1 m/s at -800 V. Measurements along the other two axes, much like the velocity change, are largely uninfluenced by the kick.

We compare the measured data with the results of numeric simulations of a cloud of 10^5 noninteracting particles, shown as solid lines in Fig. 3. Most of the simulation parameters are set near the experimental parameters, but the initial cloud location and width as well as the pinhole location are left free. This provides a coarse model of the otherwise intricate supersonic beam dynamics. The cloud is initialized at the skimmer location using a Gaussian spatial distribution with a standard deviation of 0.25 cm transversely and 0.5 cm longitudinally. Independently, the velocities are drawn from a Maxwell distribution defined by the temperatures of 100 mK transversely and 200 mK longitudinally. The pinhole is simulated 4.0 cm closer to the skimmer than in the experiment in order to adjust the temperature and spatial-velocity correlation of the cloud at the time of the kick. The location of tagging minimally affects the simulated velocity curves shown in Fig. 3.

Finally, the data in Fig. 3 is used to estimate the one-dimensionality of our kick. As both the kick and heating along the x, y axes are negligible, we plot the ratio $\Delta v/\Delta v_{\rm th}$ for only the z axis (see Fig. 4). The horizontal dash-dotted lines indicate the threshold for quasi-one-dimensionality ($\Delta v/\Delta v_{\rm th} = \pm 1$), the point above which the kick dominates the change in the velocity profile of the cloud. These values set a lower limit on the one-dimensionality of the kick, while an exact threshold depends on the application in question. For example, magneto-optical cooling (MOP) cooling requires a minimum ratio of $\Delta v/\Delta v_{\rm th} \sim 1.6$, below which heating of the cloud during the MOP stages will dominate over the cooling efforts. For our data, the measured Δv begins to exceed $\Delta v_{\rm th}$ at $|V_{\rm bias}| \gtrsim 300$ V.

We can also discuss the appearance of an ideal one-dimensional kick for an experiment on stationary atoms by formulating a simple model that includes the experimental parameters. First, we assume that the cloud is cold ($T = 0.3$ mK) and small in size ($\sigma = 1$ mm), which approximate values for lithium released from a magneto-optical trap. It is in this setting where a one-dimensional magnetic kick is expected to be most useful. In this situation, the impulse on the cloud can be approximated as a kick $\kappa(r) = \mu\,\nabla|\mathbf{B}(\mathbf{r})|\,\tau/m$ that depends only on the position of an atom during the kick duration τ.

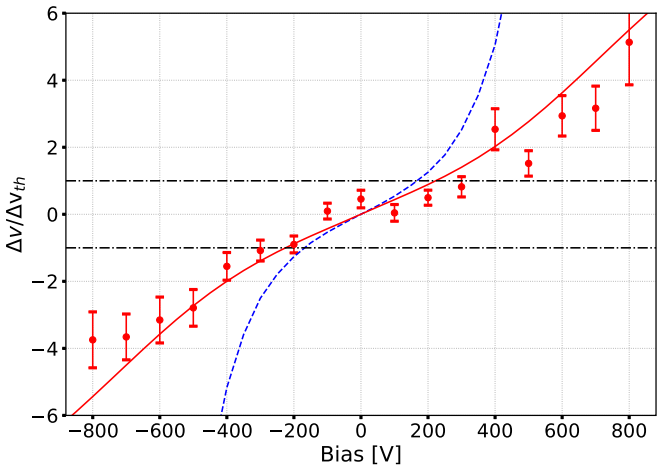

FIG. 4. Ratio of the changes in velocity and thermal velocity as a function of bias voltage. Solid red curve corresponds to simulation results, whereas the dashed blue line represents a one-dimensional kick on stationary atoms at 0.3 mK with $\sigma = 1$ mm. The black dash-dotted lines indicate the threshold for one-dimensionality.

Given this assumption, the observed velocity change Δv and heating Δv_{th} can be estimated as

$$\Delta v = \int f(r, v)\kappa(r) dr\, dv$$

and

$$\Delta v_{\text{th}} = \sqrt{\int f(r, v)[\kappa(r) - \Delta v]^2 dr\, dv}$$

where $f(r, v)$ is the joint Gaussian distribution of the position and velocity of the cloud. Using this model, we generate the expected shape of an ideal one-dimensional kick, $\Delta v/\Delta v_{\text{th}}$ versus bias voltage, shown as a dashed blue line on Fig. 4. It can be seen that the data, simulation, and model show a reduction in Δv_{th} at high bias, signifying that we are approaching the one-dimensional regime. However, given that our data have $|\Delta v/\Delta v_{\text{th}}| = 5.1 \pm 1.3$ for $+800$ V of bias and 3.7 ± 0.8 for -800 V of bias, we can only claim that we reach a quasi-one-dimensional regime. A full transition does not occur for our system mainly due to the duration of the kicking pulse compared to the propagation time of the cloud through the coils. Both timescales are comparable ($\approx 100\,\mu$s), which leads to the cloud interacting with different regions of the kicking field, including those where the kick is oriented at an angle [see, e.g., position $(x, y) = (-10\,\text{mm}, 0\,\text{mm})$ on Fig. 2(c)].

To produce a truly one-dimensional kick with minimal heating at high biases, the propagation time of the cloud in the coils must be small in comparison to the pulse width of the kick in order to minimize the end effects of the coils. At our beam velocity of 480 m/s, a kicking pulse length $\sim 10\,\mu$s would be required. While such pulse lengths can be created by reducing the coil inductances, even our pulse lengths and configurations should be able to provide a truly one-dimensional magnetic kick to a cold trapped sample rather than a moving beam. Furthermore, the quasi-one-dimensional kick can easily be extended to smaller Δv by proportional scaling of the bias and kick coil currents.

The deflection of an atomic beam by an inhomogeneous magnetic field, known as the Stern-Gerlach effect, must be accompanied by a divergence of the beam in directions other than that of the deflection. By using pulsed electromagnets to provide a magnetic field gradient plus a bias, we are able to maximize deflection and minimize the accompanied heating of our supersonic lithium beam. We have presented a quantitative experimental study of the dimensionality of the Stern-Gerlach effect as a function of the applied bias.

Our results, which are supported by numeric simulations of particle trajectories, illustrate a regime in which the deflection dominates the spreading. Hence, we realize a quasi-one-dimensional Stern-Gerlach effect. Such an effect has applications in spatial separation and guidance of atomic beams. Using a model valid for colder trapped samples, we predict the same technique can provide a near-perfect one-dimensional kick to the system. True one-dimensional kicks on cold trapped samples will enable new methods of phase space compression like MOP cooling. Unlike the established method of evaporative cooling, the one-dimensional kicks of MOP cooling conserve atom number through the cooling process, one day leading to larger samples of quantum degenerate gases.

Our method of one-dimensional kicks could be adapted to simulate microgravity conditions by replacing pulses with fixed currents. To levitate a cloud of lithium atoms of 1 mm in size, we estimate the required field gradient and bias to be 12 mT/m and 1.25 T, respectively. Both of these values are well within an experimentally achievable setup if superconducting magnets are considered. Creation of force-free regions over the range of a few millimeters will allow for Earth-bound experiments that operate at the same level of gravity cancellation as present on the International Space Station [18].

This work was supported by funding from the W. M. Keck Foundation. We would also like to thank Dmitry Budker and Simon Rochester for valuable discussions.

[1] M. O. Scully, W. E. Lamb, and A. Barut, Found. Phys. **17**, 575 (1987).
[2] W. Gerlach and O. Stern, Z. Phys. **8**, 110 (1922).
[3] T. M. Roach, H. Abele, M. G. Boshier, H. L. Grossman, K. P. Zetie, and E. A. Hinds, Phys. Rev. Lett. **75**, 629 (1995).
[4] K. S. Johnson, M. Drndic, J. H. Thywissen, G. Zabow, R. M. Westervelt, and M. Prentiss, Phys. Rev. Lett. **81**, 1137 (1998).
[5] E. A. Hinds and I. G. Hughes, J. Phys. D: Appl. Phys. **32**, R119 (1999).
[6] P. Rosenbusch, B. V. Hall, I. G. Hughes, C. V. Saba, and E. A. Hinds, Phys. Rev. A **61**, 031404(R) (2000).

[7] D. Kadio, O. Houde, and L. Pruvost, Europhys. Lett. **54**, 417 (2001).
[8] J. Gardner, R. Castillo-Garza, and M. G. Raizen, J. Chem. Phys. **139**, 096103 (2013).
[9] J. R. Gardner, E. M. Anciaux, and M. G. Raizen, J. Chem. Phys. **146**, 081102 (2017).
[10] S. Machluf, Y. Japha, and R. Folman, Nat. Commun. **4**, 9 (2013).
[11] Y. Margalit, Z. Zhou, O. Dobkowski, Y. Japha, D. Rohrlich, S. Moukouri, and R. Folman, arXiv:1801.02708.
[12] T. R. Mazur, B. Klappauf, and M. G. Raizen, Nat. Phys. **10**, 601 (2014).
[13] D. Dreon, L. A. Sidorenkov, C. Bouazza, W. Maineult, J. Dalibard, and S. Nascimbene, J. Phys. B **50**, 065005 (2017).
[14] M. G. Raizen, D. Budker, S. M. Rochester, J. Narevicius, and E. Narevicius, Opt. Lett. **39**, 4502 (2014).
[15] Y. Li, G. Feng, R. Xu, X. Wang, J. Wu, G. Chen, X. Dai, J. Ma, L. Xiao, and S. Jia, Phys. Rev. A **91**, 053604 (2015).
[16] D. Becker, M. D. Lachmann, S. T. Seidel, H. Ahlers, A. N. Dinkelaker, J. Grosse, O. Hellmig, H. Müntinga, V. Schkolnik, T. Wendrich *et al.*, Nature (London) **562**, 391 (2018).
[17] R. Senaratne, S. V. Rajagopal, Z. A. Geiger, K. M. Fujiwara, V. Lebedev, and D. M. Weld, Rev. Sci. Instrum. **86**, 023105 (2015).
[18] K. Jules, K. McPherson, K. Hrovat, E. Kelly, and T. Reckart, Acta Astronaut. **55**, 335 (2004).